Solid State Communications 177 (2014) 36–41

Contents lists available at ScienceDirect

Solid State Communications

journal homepage: www.elsevier.com/locate/ssc

Effects of ferromagnetic nanopillars on spin coherence in an InGaAs quantum well

Yao Zhang, J.J. Heremans *

Department of Physics, Virginia Tech, Blacksburg, VA 24061, USA

ARTICLE INFO

Article history:
Received 28 July 2013
Received in revised form
23 August 2013
Accepted 13 September 2013
by G.E.W. Bauer
Available online 7 October 2013

Keywords:
A. Quantum wells
B. Electron beam lithography
D. Antilocalization
E. Magnetotransport

ABSTRACT

Low-temperature antilocalization measurements are used to investigate the interactions between a two-dimensional electron system in an $In_{0.53}Ga_{0.47}As$ quantum well in an InGaAs/InAlAs heterostructure, and the magnetic moments of CoFe nanopillars located on the heterostructure surface. With CoFe nanopillars, a decrease in spin coherence time is observed, attributed to the spatially varying magnetic field from the local moments. A good agreement between the data and calculations suggests that the CoFe nanopillars also generate an appreciable average magnetic field normal to the surface of value ~35 G at the quantum well. The measurements further show that surface metal coverage increases mobility, and for non-magnetic coverage increases spin coherence time, consistent with the Elliott–Yafet spin-decoherence mechanism. Phase coherence times decrease as the temperature decreases, consistent with phase decoherence via the Nyquist mechanism.

1. Introduction

Quantum properties of surface states and interactions between local surface moments and itinerant carriers may be probed by low-temperature antilocalization (AL) measurements [1–5]. The modification of magnetic and transport properties by surface moments is of interest because they allow access to important parameters of spintronics and quantum information processing. Recently reported was a tunable artificial structure of magnetic moments on a reduced-dimensionality electron system, where rare earth ions deposited on InAs films induce magnetic spin-flip scattering from spin-exchange interactions of the local moments with the two-dimensional surface accumulation electron layer [5]. This work investigates related interactions in a similar geometry, namely between lithographically delineated ferromagnetic CoFe nanopillars on the surface of an $In_{0.53}Ga_{0.47}As/In_{0.52}Al_{0.48}As$ heterostructure and electrons in the heterostructure's quantum well (QW). The surface CoFe nanopillars are in close proximity to the QW, distanced by approximately one Fermi wavelength.

Quantum interference of charge carriers on time reversed paths causes quantum corrections to the conductivity in low-temperature electronic transport, thereby leading to the phenomena of AL [6–8] and weak-localization (WL) [7,8]. Under a magnetic field B applied normal to the surface, constructive interference causes a negative magnetoresistance (MR), known as WL. With spin–orbit interaction (SOI), the interference is destructive and causes a turnaround to positive MR at very low B, resulting in AL. The heterostructure studied here has a prominent Rashba SOI caused by structural inversion asymmetry, and hence shows AL. The characteristic MR of AL, being due to spin-dependent quantum interference, carries quantitative information about phase and spin decoherence, and thus is a valuable tool to experimentally study the SOI spin decoherence time τ_{SO}, the inelastic scattering time τ_i, and the magnetic spin-flip scattering time τ_s. Together τ_i and τ_s determine the phase coherence time τ_ϕ as $\tau_\phi^{-1} = \tau_i^{-1} + 2\tau_s^{-1}$ [9,10]. When spin-flipping interactions between surface magnetic moments and the QW electrons can be neglected then $\tau_\phi^{-1} = \tau_i^{-1}$, which is the case for the system under study. In a series of comparative measurements we find that the presence of the ferromagnetic nanopillars modifies the SOI and phase coherence properties of the two-dimensional electron system (2DES) in the QW, as determined by the quantum corrections to the 2DES conductivity arising from AL.

2. Experiment

Using electron-beam lithography, two adjacent twin serpentine structures were patterned onto a Hall bar mesa (itself patterned on the heterostructure material), as depicted in Fig. 1(a). One serpentine is always left bare while the other is covered by lithographically fabricated nanopillars, allowing comparative measurements. The serpentines increase the signal by increasing the channel

* Corresponding author. Tel.: +1 540 231 4604.
E-mail address: heremans@vt.edu (J.J. Heremans).

0038-1098/$ - see front matter © 2013 Elsevier Ltd. All rights reserved.
http://dx.doi.org/10.1016/j.ssc.2013.09.027

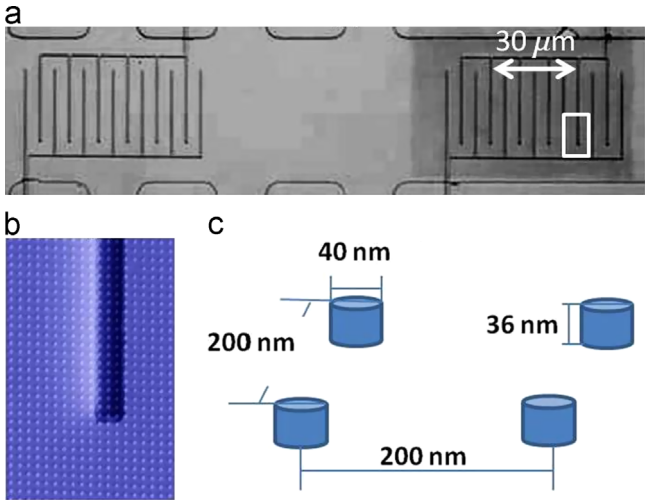

Fig. 1. (Color online) (a) Optical micrograph of a sample, with twin serpentine structures (bare and nanopillar-covered) on a mesa. The dark area (on the right) is covered by nanopillars. (b) Scanning electron micrograph of the area within the white outline in (a). (c) Dimensions of the Al/CoFe nanopillars and their array in (b).

length (440 μm) to width (5 μm) ratio. An array of ferromagnetic nanopillars was delineated by thermal evaporation and lift-off after electron-beam lithography [Fig. 1(b) and (c), where dimensions are indicated]. Each pillar consists of two layers, a 7 nm thick non-magnetic Al adhesion layer and a 29 nm thick ferromagnetic $Co_{0.6}Fe_{0.4}$ layer. The sample carrying one bare serpentine and one serpentine covered with Al/CoFe nanopillars will be called the Al/CoFe sample. To assess the influence of the Al adhesion layer on the measurements, a control sample with one bare serpentine and one covered by an array of 9 nm Al nanopillars is also fabricated (called the Al sample; the Al array has dimensions identical to the Al/CoFe array). Apart from the presence of the nanopillars, the twin serpentines on one sample experience the same fabrication processes and are together cooled down to the experiment temperature T (0.4 K and 1.3 K), allowing comparative measurements to assess the influence of the nanopillars [5]. Magneto-transport measurements were conducted using standard four-contact low-frequency lock-in techniques. Prior to discussing heterostructure properties and to show the effect of the nanopillars, the comparative low-B AL data for the Al/CoFe sample and the Al sample at two temperatures is represented in Fig. 2. The AL correction to the longitudinal resistance R is defined as $\Delta R(B) = R(B) - R_0$, where $R_0 = R(B=0)$. To account for contributions from the Hall effect or other slight electronic shifts, the antisymmetric component has been subtracted from the data. The data displayed in Fig. 2 exhibits the characteristic shape of AL, with an initial increase in R from $B=0$, reaching a maximum at $B \sim 90$ G, beyond which negative MR is observed. The separation in B between two resistance maxima scales with τ_{SO}^{-1}, while the depth of the resistance minimum scales with the ratio τ_ϕ/τ_{SO} (detailed fits are presented later). In Fig. 2(a) and (c) we plot the MR of the *bare* serpentines of both the Al/CoFe sample and the Al sample (to account for processing variations between the samples, we scale the resistance values of the Al sample by a multiplier of 1.5, which does not influence the τ_ϕ and τ_{SO} values deduced from the data). In Fig. 2(b) and (d) we plot the MR of the serpentines *covered* with nanopillars of both the Al/CoFe sample and the Al sample. From Fig. 2(a)–(d), evaluating the data for the Al sample (black traces), it is apparent that Al nanopillars lower, but do not broaden the AL signal. In contrast, the Al/CoFe nanopillars not only lower the AL signal, they notably broaden the shape as well, demonstrating the sensitivity of AL to surface coverage [5]. Information about the interaction between the surface moments and the 2DES is extracted from the comparative (rather than absolute) AL data, as described below.

The InGaAs 2DES schematically depicted in Fig. 3 was grown by molecular-beam epitaxy on semi-insulating InP (001) substrate. The heterostructure consists of a 500 nm $In_{0.52}Al_{0.48}As$ buffer, a 6 nm $In_{0.52}Al_{0.48}As$ doping layer, a 7 nm $In_{0.52}Al_{0.48}As$ layer, the 10 nm wide $In_{0.53}Ga_{0.47}As$ QW, a 17 nm $In_{0.52}Al_{0.48}As$ layer, and a 2 nm undoped InP cap layer. The transverse (R_{XY}) and longitudinal (R_{XX}) transport coefficients shown in Fig. 3 are employed to characterize the transport properties of the samples. Hall effect (R_{XY}) and Shubnikov–De Haas oscillations (R_{XX}) are in accordance with concerning the 2DES areal density N_s. The coefficients show that no evidence of two-band transport and single-subband occupancy is thus assumed. Accounting for nonparabolicity in the InGaAs conduction band, with a Γ-point ratio of effective mass to free-electron mass of 0.0353 and a low T band gap of 813 meV, the measured N_s and mobilities μ are used to derive other transport parameters, such as the elastic scattering time τ_0 and the two-dimensional diffusion constant D. Table 1 summarizes the properties at $T=0.4$ K. N_s and μ do not vary between $T=0.4$ K and 1.3 K. As Table 1 indicates, we experimentally find that the Al/CoFe or Al nanopillar coverage tends to increase N_s and μ. With the nanopillars covering $\sim$ 3% of the surface, the increase in N_s and μ can be attributed either to a change in Fermi level pinning and band bending at the surface (changing N_s and hence μ in the QW), or to increased Coulombic screening by the presence of an effectively metallic coverage, or both. Compared with the other $In_{0.53}Ga_{0.47}As/In_{0.52}Al_{0.48}As$ heterostructures [11,12], the values of μ of the present 2DES are lower, due to the single doping layer situated underneath the QW. While this feature reduces μ, it ensures a strong asymmetry of the confinement potential and hence substantial SOI exploited in this work for the pronounced AL to which it leads.

3. Analysis and results

The AL quantum corrections to the two-dimensional conductivity $\sigma_2(B)$ are sensitive to τ_0, τ_ϕ, τ_s, and τ_{SO}. An expression for $\Delta\sigma_2(B) = \sigma_2(B) - \sigma_2(B=0)$ is obtained as [6,16]

$$\Delta\sigma_2(B) = \frac{e^2}{2\pi^2\hbar}\left\{-\left[\psi\left(\frac{1}{2}+\frac{B_0}{|B|}\right)-\psi\left(\frac{1}{2}+\frac{B_\phi+B_{SO}-B_s}{|B|}\right)+\frac{1}{2}\psi\left(\frac{1}{2}+\frac{B_\phi}{|B|}\right)-\frac{1}{2}\psi\left(\frac{1}{2}+\frac{B_\phi+2B_{SO}-2B_s}{|B|}\right)\right]+\left[\ln\left(\frac{B_0}{|B|}\right)-\ln\left(\frac{B_\phi+B_{SO}-B_s}{|B|}\right)+\frac{1}{2}\ln\left(\frac{B_\phi}{|B|}\right)-\frac{1}{2}\ln\left(\frac{B_\phi+2B_{SO}-2B_s}{|B|}\right)\right]\right\}, \quad (1)$$

where $\psi(x)$ is the digamma function and the characteristic fields are defined as $B_0 = \hbar/(4eD\tau_0)$, $B_\phi = \hbar/(4eD\tau_\phi)$, $B_{SO} = \hbar/(4eD\tau_{SO})$, and $B_s = \hbar/(4eD\tau_s)$. Considering $\Delta R(B) \ll R_0$, Eq. (1) can be directly compared with the experimental $\Delta R(B)/R_0$ values through $\Delta\sigma_2(B)/\sigma_2(B=0) \approx -\Delta R(B)/R_0$. Good correspondence exists between Eq. (1) and our experimental results. While Eq. (1) is parameterized in B_0, B_ϕ, B_{SO}, and B_s, only B_ϕ, B_{SO}, and B_s have to be obtained from a least-squares fit or other considerations, since B_0 can be derived from the transport parameters τ_0 and D.

On the bare serpentines of the Al/CoFe sample and of the Al sample, and on the Al nanopillar-covered serpentine of the Al sample, no magnetic species are introduced, and thus $B_s \to 0$. We expect the two bare serpentines (Fig. 2 (a) and (c)) to yield similar τ_ϕ and τ_{SO} values and indeed when we perform a least-squares fitting and extract τ_ϕ and τ_{SO} for the Al/CoFe sample and the Al

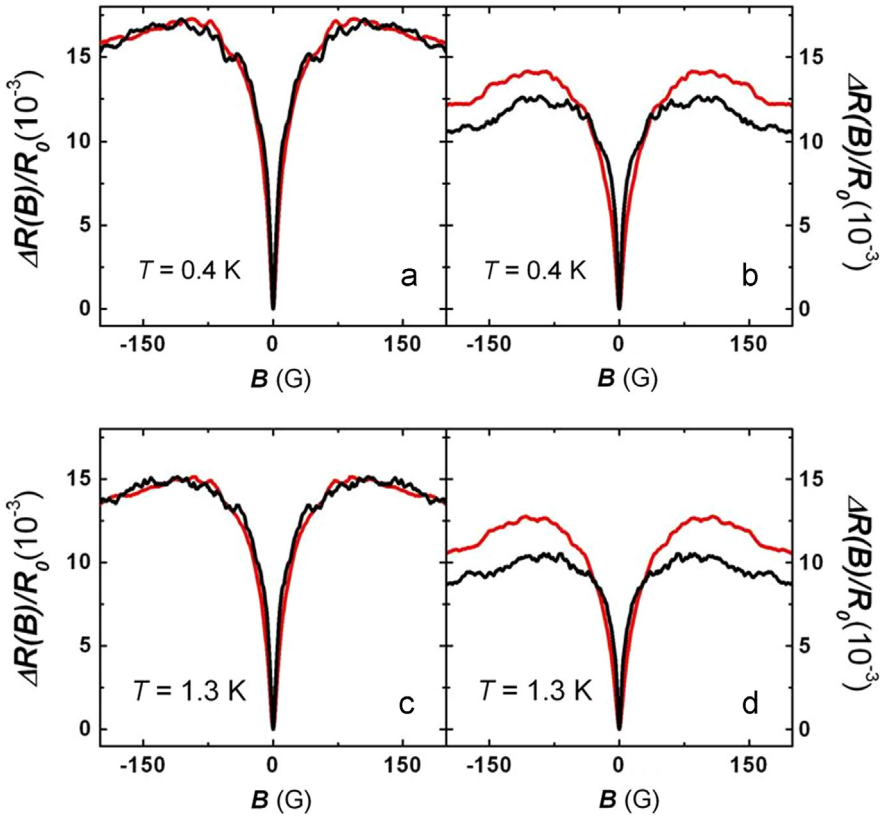

Fig. 2. (Color online) (a) Magnetoresistance due to AL at 0.4 K on the bare serpentines of the Al/CoFe sample (red) and the Al sample (black). (b) Magnetoresistance due to AL at 0.4 K of nanopillar-covered serpentines of the Al/CoFe sample (red) and the Al sample (black). (c) Same as (a) but at 1.3 K. (d) Same as (b) but at 1.3 K.

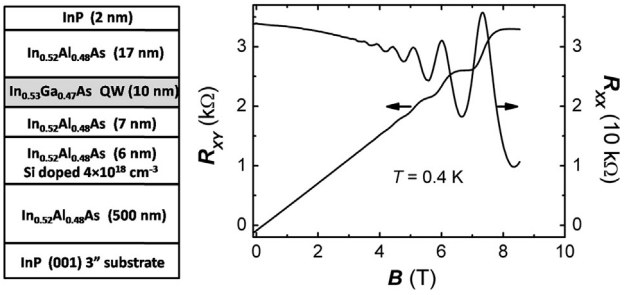

Fig. 3. Left panel: Schematic of the InGaAs/InAlAs heterostructure, with the quantum well (shaded) located 19 nm below the surface. Right panel: R_{XY} and R_{XX} transport coefficients vs B, obtained on the bare serpentine of the Al sample at 0.4 K.

Table 1
2DES serpentine transport properties: N_s, μ, and D, at T=0.4 K.

	Al/CoFe sample		Al sample	
Property	Covered	Bare	Covered	Bare
N_s (10^{12} cm^{-2})	1.6	1.5	1.7	1.6
μ (10^4 cm^2/V s)	0.68	0.63	1.2	1.0
D (10^3 cm^2/s)	1.1	0.91	2.0	1.6

sample, we find that τ_ϕ and τ_{SO} values for both bare serpentines are close: both τ_ϕ and τ_{SO} of the Al/CoFe sample are 1.2 times higher than that of the Al sample. A fitting for the Al nanopillar-covered serpentine of the Al sample also yields values for its τ_ϕ and τ_{SO}. Values are tabulated as scattering rates in Table 2. We now turn to the Al/CoFe nanopillar-covered serpentine of the Al/CoFe sample. From previous studies of magnetic impurities in metal

Table 2
2DES scattering rates and fitting parameters: τ_0^{-1}, τ_i^{-1}, τ_{SO}^{-1} and $|\overline{B_z}|$, at T=0.4 K and 1.3 K.

	Al/CoFe sample		Al sample	
Parameter	Covered	Bare	Covered	Bare
τ_0^{-1} (ps^{-1})				
(0.4 K)	2.5	2.7	1.4	1.8
(1.3 K)	2.5	2.7	1.4	1.8
τ_ϕ^{-1} (ps^{-1})				
(0.4 K)	0.10	0.077	0.081	0.063
(1.3 K)	0.27	0.21	0.22	0.17
τ_{SO}^{-1} (ps^{-1})				
(0.4 K)	0.91	0.77	0.48	0.63
(1.3 K)	0.91	0.77	0.48	0.63
$\lvert\overline{B_z}\rvert$ (G)				
(0.4 K)	34	–	–	–
(1.3 K)	36	–	–	–

systems [1], we learn that ferromagnetic nanopillars can influence the spin-flip scattering rate τ_s^{-1} and induce an additional spin–orbit scattering rate τ_{SO}^{-1}, without affecting the inelastic scattering rate τ_i^{-1}. Yet, a test fitting for the Al/CoFe nanopillar-covered serpentine indicates that B_s is at least two orders of magnitude smaller than B_ϕ and B_{SO}, and thus negligible. This finding is not unexpected, since spin-flip scattering requires an exchange mechanism between the 2DES and the ferromagnetic pillars, repressed by the 26 nm separation between the 2DES and the ferromagnetic species. The spatially varying fringing magnetic fields from the ferromagnetic pillars (quantified below) are not expected to lead to spin-flip scattering. Yet, we experimentally

find that the fringing fields affect the AL data by generating an average offset in the value of B normal to the surface, with a constant offset absolute value $|\overline{B_z}|$ and a sign following the sign of the applied B. A good fit is obtained when introducing $|\overline{B_z}|$ as an additional fitting parameter. Indeed, each Al/CoFe nanopillar is magnetized by the external B and accordingly generates a fringing field, which can be estimated. The saturation magnetization of $Co_{0.6}Fe_{0.4}$ can be calculated from superconductor–insulator–ferromagnet spin polarization data [13], as $M_s = 1770$ emu/cm^3, close to the calculated saturation magnetization of $Co_{0.5}Fe_{0.5}$, $M_s = 1800$ emu/cm^3 [14]. The typically high M_s of $Co_{0.6}Fe_{0.4}$ yields fringing fields still appreciable at the QW. The fringing fields flip direction according to the direction of the applied B, and at a low coercive field. The coercive field can be estimated to be below $\sim$1 G, as a consequence of the low crystalline coercive field of the soft-magnetic $Co_{0.6}Fe_{0.4}$ ($\sim$0.2 G) [15] and the low shape anisotropy of the nanopillars (the ratio of height to diameter is 0.9). The nanopillar diameter is also small (40 nm) compared to the interpillar distance (200 nm) and hence the interaction between nanopillars is negligible. Compared with the range of B for the AL signal, the applied B where the fringing fields flip sign is thus small. The averaged contribution from the fringing fields at the level of the 2DES is then approximated as a step function described as $|\overline{B_z}|$ at $B \geq 0$, and $-|\overline{B_z}|$ at $B < 0$. The AL correction to conductivity in normal B is then modified as

$$\Delta\sigma_2'(B) = \begin{cases} \Delta\sigma_2(B+|\overline{B_z}|) - \Delta\sigma_2(|\overline{B_z}|), & B \geq 0 \\ \Delta\sigma_2(B-|\overline{B_z}|) - \Delta\sigma_2(|\overline{B_z}|), & B < 0 \end{cases}. \quad (2)$$

By fitting Eq. (2) to the AL data of the Al/CoFe nanopillar-covered serpentine, $|\overline{B_z}|$ is found to be $\sim$ 35 G (Table 2). It will be shown below that $|\overline{B_z}| \sim$ 35 G is in good agreement with a micromagnetics calculation using a magnetization normal to the 2DES plane. With a low crystalline coercive field and low shape anisotropy, anisotropy is not expected to be decisive in determining the magnetization direction, but rather the direction will depend on the orientation of the variable externally applied B, down to the very low coercive fields. For the micromagnetics calculation supporting the AL analysis we hence assume a magnetization normal to the 2DES plane. The same fitting provides B_{SO} and hence τ_{SO} for the Al/CoFe nanopillar-covered serpentine. Concerning B_ϕ and τ_ϕ, since on this serpentine $B_s \sim 0$, we have assumed the same ratio 1.2 as between the bare serpentines, between τ_ϕ of the Al/CoFe nanopillar-covered serpentine and τ_ϕ of the Al nanopillar-covered serpentine. By this method τ_ϕ and τ_{SO} are obtained for all serpentines, bare and covered, presented as scattering rates in Table 2.

4. Discussion

Fig. 4 shows the good correspondence between data and theoretical fits for both bare and covered serpentines of the two samples at different T. Different AL models and uncertainty in the transport parameters can lead to a variation of $\sim$ 30% in the absolute values of τ_ϕ and τ_{SO}. However, our experiments are comparative: we maintain the same nanopillar coverage, compare covered serpentines to bare serpentines measured on the same samples and at the same T, and apply the same model, ensuring that comparisons between covered and bare serpentines regarding τ_ϕ and τ_{SO} which bear reliable conclusions. The use of Eq. (2) results in a good fit, and is appropriate for samples where spin scattering is dominated by the Elliott–Yafet mechanism [18–21], which, as described below, will prove to be the case in our InGaAs QW.

The values in Table 2 indicate a phase decoherence rate τ_ϕ^{-1} scaling with T for each serpentine, consistent with dominant Nyquist decoherence [17] arising from fluctuations in the electromagnetic background. Experimentally, the presence of Al/CoFe or Al nanopillars increases τ_ϕ^{-1}. At low T the spin scattering of III–V narrow gap semiconductors with low μ is dominated by the Elliott–Yafet mechanism [18–21], which causes the spin–orbit scattering rate τ_{SO}^{-1} to decrease as μ increases ($\tau_{SO}^{-1} \sim \tau_0^{-1}$) [22]. We have mentioned that the Al coverage on the Al sample surface increases μ, possibly by a change in band bending or by additional screening of the ionized impurities within the heterostructure, or both. Accordingly, for the Al sample Table 2 shows a decrease in τ_{SO}^{-1} for the Al nanopillar-covered serpentine compared with the bare serpentine. The ratios between bare and covered serpentines of respective values of τ_{SO}^{-1} as well as τ_0^{-1} are both $\sim$ 1.3, showing that the Elliott–Yafet expectation of $\tau_{SO}^{-1} \sim \tau_0^{-1}$ holds for the Al sample. For the Al/CoFe sample however this relation does not hold, and the spin–orbit scattering rate τ_{SO}^{-1} increases with Al/CoFe nanopillar coverage compared to the bare serpentine. This can be explained by the fact that in addition to the average offset field $|\overline{B_z}|$, the ferromagnetic nanopillars also create a spatially varying component to the fringing field. We surmise that the varying component is sensed by the 2DES electron spins as a random spin–orbit field. SOI is experienced by electrons as an effective momentum-dependent vector potential, creating an effective magnetic field B_{eff}, in the plane of the 2DES in the case of Rashba SOI [23]. Momentum scattering (quantified by τ_0^{-1}) causes a random component to B_{eff}, and the variation in spin precession along the random component causes decoherence between spins, which in the Elliott–Yafet mechanism is not mitigated by motional narrowing as in the D'yakonov–Perel mechanism [24], and hence increases τ_{SO}^{-1} [25]. Under Al/CoFe nanopillar coverage, electron spins experience an effectively random component of the fringing field, similarly leading to precessional spin decoherence and mimicking SOI-induced spin scattering. Ultimately, the screening effect is counteracted by the effective random component of B, and we observe τ_{SO}^{-1} increasing under the Al/CoFe nanopillars. Table 2 also indicates that for both bare and covered serpentines τ_{SO}^{-1} stays constant with T, consistent with previous discussions [19].

The experiments suggest that the Al/CoFe nanopillars create a non-negligible B at the level of the 2DES, and calculations bear this out, as outlined below. We approximate each nanopillar as an ellipsoidal ferromagnetic single-domain particle at the saturation magnetization, with a demagnetization factor $\alpha = 5.30$, and with magnetization normal to the 2DES plane. Exactly below the pillar, the fringing field of one pillar is calculated to be $(4\pi - \alpha)M_s =$ 11 000 G, a substantial value. Yet, considering the distance between the 2DES and the pillars, the fringing field will fan out greatly towards the 2DES, and the return fields will reduce the average value. To quantitatively estimate $|\overline{B_z}|$ at the middle of the QW layer, each pillar is represented by a magnetic dipole positioned at a height as depicted in Fig. 5. Each magnetic dipole has a magnetic moment $m = M_s\pi(d/2)^2 t = 6.45 \times 10^{-14}$ emu (parameters defined in Fig. 5). Then the component normal to the 2DES of the fringing field from one nanopillar can be expressed as

$$B_z(x,y) = \frac{\mu_0}{4\pi}\frac{m(2z_0^2 - x^2 - y^2)}{(x^2+y^2+z_0^2)^{5/2}}. \quad (3)$$

Neighboring nanopillars are separated by a distance $R =$ 200 nm. The average $|\overline{B_z}|$ over a square of dimensions $R \times R$ centered under each pillar can be calculated as $|\overline{B_z}| = \iint B_z(x,y)\, dx\, dy/R^2 = 54$ G. When an increasing number of nanopillars with their respective return fields is taken into account, $|\overline{B_z}|$ decreases

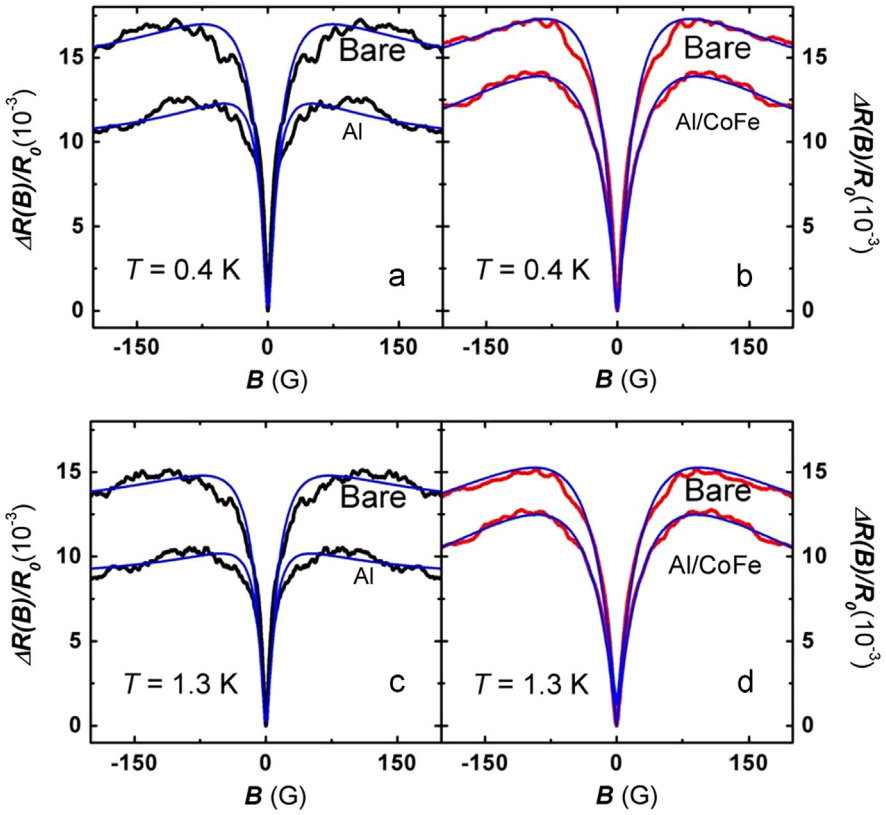

Fig. 4. (Color online) (a) Magnetoresistance due to AL on bare and covered serpentines of the Al sample (black solid lines) at $T=0.4$ K and (c) at $T=1.3$ K. (b) Magnetoresistance due to AL on bare and covered serpentines of the Al/CoFe sample (red solid lines) at $T=0.4$ K and (d) at $T=1.3$ K. Blue solid lines in all panels are theoretical fits.

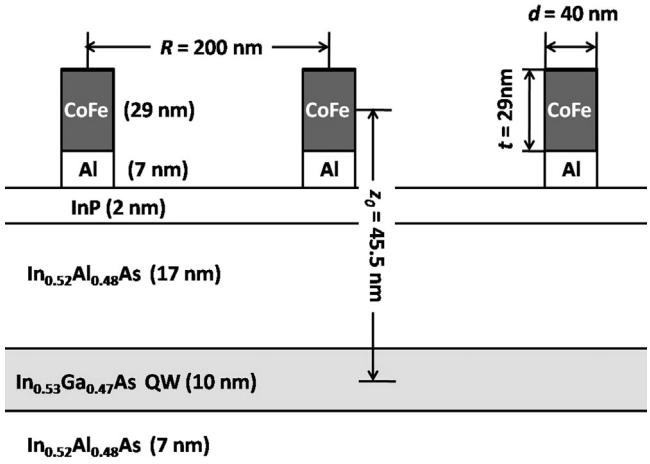

Fig. 5. Schematic side view of the Al/CoFe nanopillars on the surface of the heterostructure. The effective separation between the magnetic dipoles and the QW is taken as $z_0=45.5$ nm, the distance between two neighboring nanopillars is $R=200$ nm, the diameter of each nanopillar is $d=40$ nm, and the thickness of the CoFe layer is $t=29$ nm.

and asymptotically approaches 29 G. The value of $|\overline{B_z}|$ extracted from the AL data fits, 35 G, falls within the range found in the theoretical calculations, strongly suggesting that the magnetic fringing fields of the Al/CoFe nanopillars indeed affect our data as described.

5. Conclusion

In conclusion, using antilocalization measurements we observe interactions between two-dimensional electrons in the quantum well of an InGaAs/InAlAs heterostructure and ferromagnetic CoFe nanopillars deposited on the surface. The measurements show that the spin–orbit scattering rate is increased by the ferromagnetic nanopillars, an observation here explained by the presence of a random magnetic field component due to the fringing magnetic field of the nanopillars. On the other hand, non-magnetic Al nanopillars are observed to decrease the spin–orbit scattering rate, consistent with increased Coulombic screening under the Elliott–Yafet spin decoherence mechanism. Due to large saturation magnetization and small coercive field of the CoFe nanopillars, an average fringing field normal to the heterostructure surface has to be taken into account as well. The analysis shows that the antilocalization data is in good agreement with expectations deduced from the physics of spin–orbit interactions and simple micromagnetic models.

Acknowledgments

The authors thank R. L. Kallaher and V. Soghomonian for very useful suggestions on experiments and analysis. The research is financially supported by the U.S. Department of Energy, Office of Basic Energy Sciences, Division of Materials Sciences and Engineering under Award no. DOE DE-FG02-08ER46532.

References

[1] W. Wei, G. Bergmann, Physical Review B 37 (1988) 5990.
[2] H. He, G. Wang, T. Zhang, I. Sou, G.K. L Wong, J. Wang, H. Lu, S. Shen, F. Zhang, Physical Review Letters 106 (2011) 166805.
[3] H. Lu, J. Shi, S. Shen, Physical Review Letters 107 (2011) 076801.
[4] T. Gang, M. Deniz Yilmaz, D. Atac, S.K. Bose, E. Strambini, A.H. Velders, M.P. de Jong, J. Huskens, W.G. van der Wiel, Nature Nanotechnology 7 (2012) 232.

[5] Yao Zhang, R.L. Kallaher, V. Soghomonian, J.J. Heremans, Physical Review B 87 (2013) 054430.
[6] S. Hikami, A.I. Larkin, Y. Nagaoka, Progress in Theoretical Physics 63 (1980) 707.
[7] G. Bergmann, Physics Reports 107 (1984) 1.
[8] S. McPhail, C.E. Yasin, A.R. Hamilton, M.Y. Simmons, E.H. Linfield, M. Pepper, D.A. Ritchie, Physical Review B 70 (2004) 245311.
[9] C. Van Haesendonck, J. Vranken, Y. Bruynseraede, Physical Review Letters 58 (1987) 1968.
[10] J.C. Licini, G.J. Dolan, D.J. Bishop, Physical Review Letters 54 (1985) 1585.
[11] T. Matsuoka, E. Kobayashi, K. Taniguchi, C. Hamaguchi, S. Sasa, Japanese Journal of Applied Physics 29 (1990) 2017.
[12] E. Diez, Y.P. Chen, S. Avesque, M. Hilke, E. Peled, D. Shahar, J.M. Cerveró, D.L. Sivco, A.Y. Cho, Applied Physics Letters 88 (2006) 052107.
[13] D.J. Monsma, S.S.P. Parkin, Applied Physics Letters 77 (2000) 720.
[14] D.V. Berkov, Physical Review B 83 (2011) 054420.
[15] R.M. Bozorth, Ferromagnetism, IEEE Press, Piscataway, NJ, 1993.
[16] S.V. Iordanskii, Yu.B. Lyanda-Geller, G.E. Pikus, JETP Letters 60 (1994) 206.
[17] B.L. Altshuler, A.G. Aronov, D.E. Khmelnitsky, Journal of Physics C: Solid State Physics 15 (1982) 7367.
[18] R.J. Elliott, Physical Review 96 (1954) 266;
Y. Yafet, in: F. Seitz, D. Turnbull (Eds.) Solid State Physics, vol. 14, Academic Press, New York, 1963.
[19] R.L. Kallaher, J.J. Heremans, Physical Review B 79 (2009) 075322.
[20] P.H. Song, K.W. Kim, Physical Review B 66 (2002) 035207.
[21] J.N. Chazalviel, Physical Review B 11 (1975) 1555.
[22] M.M. Glazov, E.Ya. Sherman, V.K. Dugaev, Physica E 42 (2010) 2157.
[23] T.P. Pareek, P. Bruno, Physical Review B 65 (2002) 241305R.
[24] M.I. D'yakonov, V.I. Perel, Soviet Physics, Journal of Experimental and Theoretical Physics 33 (1971) 1053.
[25] I. Zutic, J. Fabian, S. Das Sarma, Review of Modern Physics 76 (2004) 323.